IEEE Open Journal of Nanotechnology

Received 14 August 2023; revised 23 October 2023; accepted 24 October 2023. Date of publication 27 October 2023; date of current version 17 November 2023. The review of this paper was arranged by Associate Editor Yoshiaki Kanamori.

Digital Object Identifier 10.1109/OJNANO.2023.3327997

Sputtering Deposition With Low Cost Multi-Element Powder Targets

TAMIKO OHSHIMA

Electrical and Electronic Engineering Program, School of Engineering and Graduate School of Engineering, Nagasaki University, Nagasaki City 852-8521, Japan

This work was supported by JSPS KAKENHI under Grant JP20K03921.

ABSTRACT Compared to solid target, powder target is low cost and can be varied in wide range of elemental combinations. Transparent and conductive aluminum-doped zinc oxide (AZO) thin films were prepared by sputter deposition using a mixed powder target consisting of zinc oxide and aluminum oxide powders at 98:2 wt%. The bulk density of the powder target can be varied depending on the pressing pressure. Therefore, AZO thin films were prepared on Si and sapphire substrates using powder targets with different bulk densities (ρ_{powder}) ranging from 0.898 to 3.00 g/cm^3. The fabricated structural, electrical, and optical properties of the AZO thin films were examined, and the relationships between the target bulk density and film properties were investigated. X-ray diffraction measurements revealed c-axis ZnO (002) diffraction peaks, corresponding to crystallite growth oriented perpendicular to the substrate. Hall effect measurements showed n-type conductivity, with carrier density and Hall mobility increasing as the bulk density of the powder target increased. At $\rho_{powder} = 3.00$ g/cm^3, the AZO thin film on the Si substrate showed the lowest resistivity of 1.35×10^{-3} Ω·cm. UV-visible spectroscopy measurements showed that the average transmittance in the visible light region exceeded 80% for the AZO thin films on the sapphire substrates. The figure of merit was calculated as a measure of the potential application in optoelectronic devices, resulting in 6.37×10^{-3} Ω^{-1} for $\rho_{powder} = 3.00$ g/cm^3. This research contributes to Nagasaki University's goal of "planetary health".

INDEX TERMS Aluminum-doped zinc oxide, powder target, sputtering, thin film.

I. INTRODUCTION

In November 2021, the 26th UN Climate Change Conference of the Parties was held in Glasgow, Scotland, U.K.. One of the most important themes of the conference was the reduction of greenhouse gas emissions (decarbonization), such as carbon dioxide. As countries work to realize a decarbonized society, they are increasingly moving away from gasoline-powered vehicles in favor of battery electric vehicles (BEV), and thus, the global market for BEVs is expected to expand rapidly in the future. All-solid-state lithium-ion batteries (ASSLB) are expected to solve the issues of BEV range performance, safety, lifespan, and cost. To fabricate practical ASSLBs, it is necessary to search for materials that can serve as chemically stable solid electrolytes with high ion conductivity. Solid electrolyte materials include Li metal oxide and Li metal sulfide, which are composed of three to five elements, with a large number of elemental combinations and composition ratios [1], [2]. In addition, conventional material exploration in each application field is already approaching its limit, and it is necessary to expand the scope of exploration to unknown compounds [3], [4]. However, a bottleneck in the search for new materials is the exponential increase in search time as the number of elements increases. One method that enables the rapid experimental investigation of thin film materials is sputter deposition, in which the powder is used as the target (powder sputtering). Using powder as the sputtering target allows the composition ratio of the target elements to be set freely and widely and allows the search for composite thin film materials at lower cost and faster than, for example, methods using compound solid targets or multiple simultaneous sputtering. In other words, this research method can dramatically accelerate the research and development of novel thin film materials and significantly reduce development costs.

In the sputtering method, a solid target is generally used as the base material of the thin film, but it is difficult to fabricate a solid target for materials with low melting points because a high-temperature, high-pressure environment is required to fabricate a solid target. Furthermore, for compound

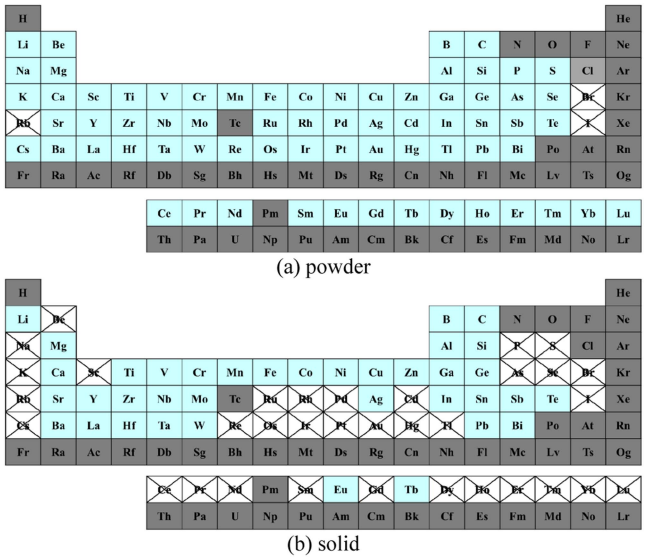

FIGURE 1. Comparison of available powders and solids as targets for sputtering. Light blue indicates an available element. ⊠indicates elements that are not available. Elements shown in gray are not sold.

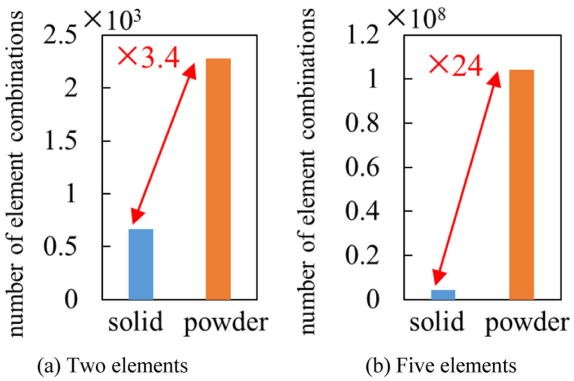

FIGURE 2. Number of combinations of in compounds with (a) two elements and (b) five elements.

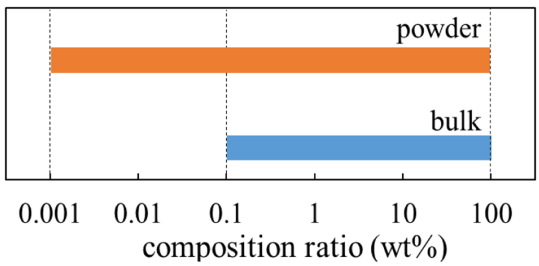

FIGURE 3. Compositional ratio range of multi-element compounds.

materials, it is time-consuming and costly to fabricate new targets by changing elemental combinations and composition ratios. Thus, powder sputtering is an efficient alternative because powder targets can be easily fabricated by simply mixing multiple types of powders. For example, this enables production of thin films using low-melting-point organic light-emitting diode (OLED) materials. In addition, when comparing targets of the same type and size, the cost of the powder was reduced to 1/1000 of that of solid materials [5], [6]. However, only a few examples of powder targets have been reported, and thus, the details of powder sputtering performance remain relatively unclear [7]. Research has gradually progressed in recent years because of the unique advantages described above [8].

This article first explains the advantages of using powder as a target in the sputtering method (Section II). Next, the author shows how to prepare mixed powder targets consisting of multiple elements and how to deposit thin films by the sputtering method (Section III). Finally, experimental results and a discussion of the fabricated thin films are presented (Section IV).

II. FEATURES OF POWDER TARGETS

A. EASE OF AVAILABILITY

The periodic table in Fig. 1 shows the elements in (a) powder and (b) solid form that can be purchased as sputtering targets by manufacturers that produce and sell thin film materials. All elements sold as single elements and in compound form were included. As search criteria, for (a), those sold in powder form were considered acceptable, while grains and masses were not. In (b), targets sold in the form of sputtering targets were accepted, but not chips, tablets, or sheets. As a result, 68 elements in (a) powder form and 37 elements in (b) solid form were available for purchase out of the 71 available elements, indicating that the powder form was 1.8 times more available than the solid form for more types of elements.

B. WIDE VARIETY OF ELEMENTAL COMBINATIONS

Compound solar cells consisting of ternary and quaternary elements are being actively researched and developed to replace non-silicon solar cells [9]. In the future, the number of elemental combinations will differ greatly between solid targets and powders for the fabrication of multi-element compounds such as quintet and hexa-element compounds. Fig. 2 compares the number of elemental combinations for (a) binary and (b) quinary compounds using the solid targets and powders available in Fig. 1. The number of elemental combinations increases dramatically as the complexity of a compound (the number of elements) increases, and data can be obtained for a very large number of elemental combinations in powders.

C. HIGHLY FLEXIBLE COMPOSITION RATIO CONTROL

A typical digital scale used to measure the amount of powder mixture has an accuracy of 0.01 g. Therefore, when the minimum mixing amount is 0.01 g, the composition ratio range of compounds using powders can be roughly estimated to be 0.001 at% at the lowest, as shown in Fig. 3, which expands the potential search range with a higher degree of freedom in the composition ratio compared with that for solids.

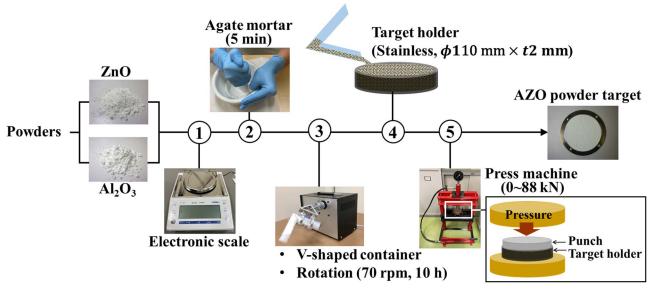

FIGURE 4. AZO mixed powder target preparation.

III. EXPERIMENTAL SETUP

A. ALUMINUM-DOPED ZINC OXIDE

Transparent conductive materials were used as powder targets for sputtering deposition in this study. Transparent conductive thin films have been used in a wide range of applications as electrodes for smartphone displays, touch panels, and solar cells, and the market has expanded along with their development. However, indium tin oxide (ITO), based on a rare metal, is expensive, difficult to supply stably, and harmful to the human body [10]. Therefore, as an alternative material to ITO, research is actively being conducted on aluminum-doped zinc oxide (AZO), using aluminum as an impurity in zinc oxide (ZnO), which is an abundant resource and harmless to the human body [11], [12]. AZO was also chosen as the benchmark in this study because of the large amount of data available for ITO and AZO.

B. PREPARATION OF AZO POWDER TARGETS

To fabricate AZO thin films, powder targets are blended with ZnO and Al_2O_3; powders. Fig. 4 shows the preparation procedure for the AZO mixed powder target. First, powders of ZnO (particle size, 1 μm; purity, 99.99%) and Al_2O_3 (particle size, 1 μm; purity, 99.9%) are weighed using an electronic scale to obtain the desired concentrations, ZnO:Al_2O_3 = 98:2 wt%. Next, the powders are mixed lightly in an agate mortar, then placed in a homemade V-shaped container and rotated for 10 hours to mix them. Then, the target sputtering holder is filled, and the surface is flattened to complete the process. If pressing is required, a press is used to compress the powder. In this way, a mixed powder target can be made in a few steps, and the mixing ratio can be set freely by changing the weight ratio of the powders. There are multiple reports on blending ZnO with powders, such as Al_2O_3, Ga_2O_3, and SnO_2, and several reports describe the fabrication of powder targets by mixing them in a rotating drum for several hours [11], [13], [14], [15]. The bulk density of the prepared powder target was calculated from the weight and volume of the powder. Fig. 5 shows the relationship between compression pressure and bulk density. Without pressing, the powder is loosely packed and has large voids. At lower pressures, the powder rearranges and the voids are filled, leading to a high rate of density increase. Further increasing pressure causes the voids to become more densely packed, and the particles are plastically deformed, resulting in a larger contact area between particles and an increase in contact points. This increases the density, but the rate of density increase is much lower [16]. In Fig. 5, the rate of density increase is high between 0 and 60 kN of pressure, but as the pressure increases further, the rate of density increase becomes much lower. Therefore, in this study, the powder targets prepared in the region of a high rate of density increase were used.

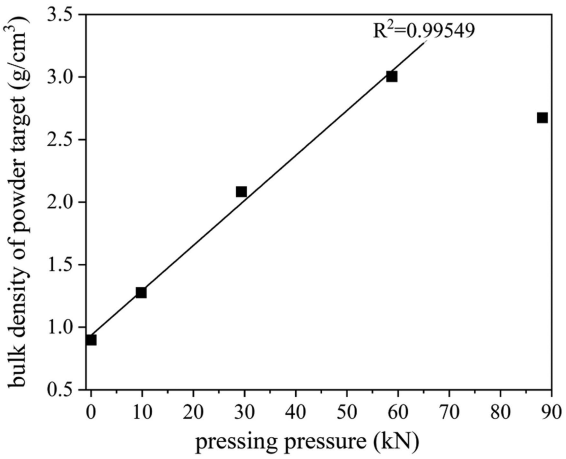

FIGURE 5. Relationship between the pressing pressure and bulk density of the fabricated powder target.

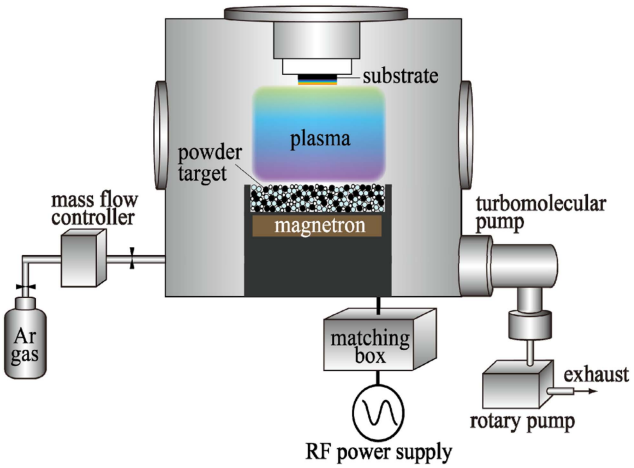

FIGURE 6. Schematic diagram of the sputtering apparatus used to prepare thin films from powder targets.

C. SPUTTERING DEPOSITION OF AZO THIN FILMS

Fig. 6 shows a schematic of the RF magnetron sputtering apparatus (Shibaura Eletec Co., EEA-04TM-sb). The AZO powder target is placed at the bottom, the substrates (silicon, sapphire) are positioned at the top and the sputter-up method is used. The experimental method is the same for solid targets. The sputtering conditions were RF power of 100 W, Ar gas pressure of 0.38 Pa, and distance between target and substrate of 68 mm. With these conditions held constant, AZO thin

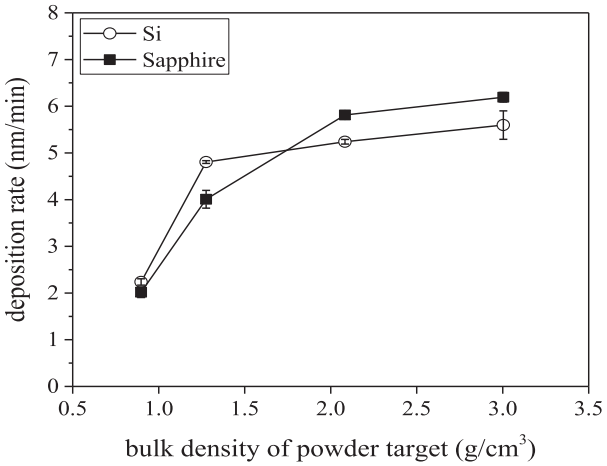

FIGURE 7. Deposition rates of AZO thin films prepared with powder targets of different bulk densities.

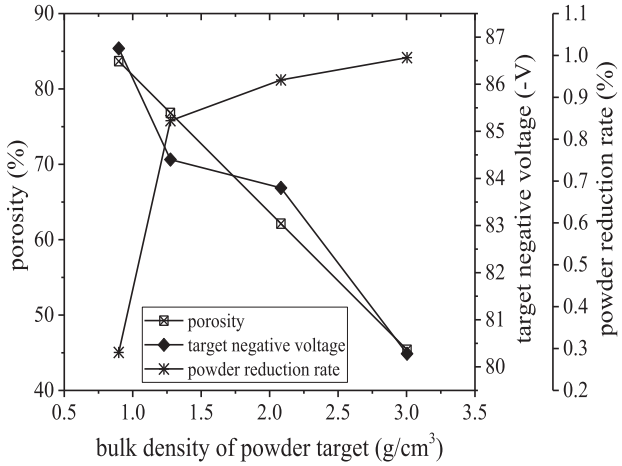

FIGURE 8. Porosity calculated from theoretical solid density and bulk density of the powder target (⊠), DC negative voltage when sputtering powder targets of different bulk densities (♦), and powder reduction rate calculated from powder target weight before and after AZO thin film fabrication (∗).

films were prepared using AZO powder targets with various bulk densities (0.898, 1.28, 2.08, 3.00 g/cm^3) and a deposition time of 60 min. The fabricated AZO thin films were evaluated using an X-ray diffractometer, UV-visible spectrophotometer, high-precision microstructure measuring machine, and Hall effect measurement system.

IV. RESULTS AND DISCUSSION

A. DEPOSITION RATE

Fig. 7 shows the deposition rate, calculated from the film thickness and the deposition time, as a function of the bulk density. The deposition rate increases as the target density increases but saturates in the middle. The deposition rate of AZO thin films fabricated with an AZO solid target and a theoretical density of 96% under almost the same conditions used in this study was 11.4 nm/min, and the maximum deposition rate obtained in the present study was approximately half that of the solid target [17]. Weighing the mass of the target before (m_1) and after (m_2) deposition, $(m_1–m_2)/m_1$ indicates the rate of reduction of the powder target caused by sputtering. The relationship between the rate of reduction and target density is shown in Fig. 8, where the rate of reduction of the powder target increases with increasing target density, which shows a saturating trend similar to the deposition rate in Fig. 7. Fig. 8 also shows the porosity of the powder target and the DC negative voltage generated in the powder target. The theoretical density ρ_{bulk} of AZO for 2% Al-doped ZnO has been defined as 5.56 g/cm^3 [18]. If the density of the mixed powder target is ρ_{powder}, the porosity is expressed as $(\rho_{bulk}–\rho_{powder})/\rho_{bulk}$. The lowest density of the mixed powder target, 0.898 g/cm^3, has 85% more porosity than the solid target because it was not pressed. It is inferred that a larger porosity results in more electrons flowing into the target and charging the blocking capacitor, which is related to an increase in the DC negative voltage [19], [20]. Considering the morphology of the target surface shown in Fig. 9(a), it is inferred that, when Ar ions

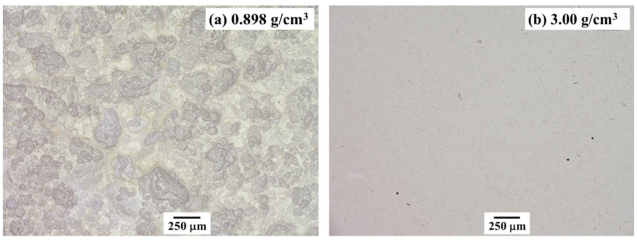

FIGURE 9. Optical micrographs of the powder target surface. .

accelerated by DC negative voltage strike the uneven target surface, the ejected particles reattach at the hills and valleys of the target, resulting in a smaller deposition rate [21]. When the target density was increased by pressing, the surface became flatter, porosity and DC negative voltage decreased, and the number of particles ejected from the target increased, which corresponds with morphology shown in Fig. 9(b). When the temperature of the target surface was measured during deposition with a radiation thermometer through the BaF_2 window, the maximum temperatures were different for both sides of Fig. 9, suggesting that the target with large porosity had a higher temperature because of poor thermal conductivity.

B. STRUCTURAL PROPERTIES

Fig. 10 shows the X-ray diffraction (XRD) measurement results of AZO thin films. The diffraction peaks of ZnO (002) and (004) were observed in all AZO thin films on both the Si and sapphire substrates, characteristic of the hexagonal wurtzite structure with preferential orientation in the c-axis, perpendicular to the substrate. Furthermore, the vertical axis scales in Fig. 10 are aligned, and comparing the peak intensities, the peak of ZnO (002) is stronger and sharper for the sapphire substrate than for the Si substrate. The crystallite

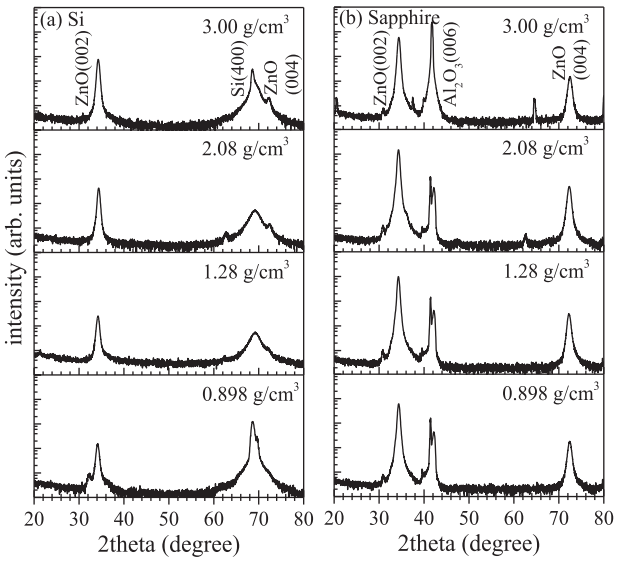

FIGURE 10. **XRD diffraction patterns of AZO thin films fabricated on (a) Si and (b) sapphire substrates using powder targets with different bulk densities.**

sizes D are calculated using Scherrer's formula

$$D = \frac{0.9\lambda}{B\cos\theta}\,(\text{nm}) \tag{1}$$

where λ, θ, and B are the X-ray wavelength, Bragg diffraction angle, and full width at half maximum (FWHM) of the ZnO (002) diffraction peak, respectively [22]. The strain ε_{zz} in the c-axis direction was determined using the biaxial strain model [23], [24].

$$\varepsilon_{ZZ} = \frac{c_{bulk} - c_{film}}{c_{bulk}} \times 100(\%) \tag{2}$$

where, c_{film} and c_{bulk} are the c-axis lattice constants for AZO thin films (calculated using the Bragg formula, $\lambda = 2d\sin\theta$) and ZnO bulk (5.207 according to the joint committee for powder diffraction standards (JCPDS) card No. 36-1451), respectively. The biaxial stress σ_{film} was related to the measured c-axis strain as follows [24], [25]:

$$\sigma_{film} = -233 \times \frac{c_{bulk} - c_{film}}{c_{bulk}}(\text{GPa}) \tag{3}$$

Table 1 summarizes the structural properties of all AZO thin films prepared on Si and sapphire substrates as a function of the powder target density ρ_{powder} using (1)–(3) and the XRD measurements in Fig. 10. Notably, the c-axis strain ε_{zz} values are negative and the biaxial stress σ_{film} values are positive. Negative values indicate compressive strain in the thin film, whereas positive values indicate tensile strain. Therefore, it is inferred that all AZO thin films prepared in this study experienced tension in the horizontal direction along the substrate surface, resulting in compressive state strain in the vertical direction normal to the substrate surface. Comparing Si and sapphire substrates, the values of ε_{zz} and σ_{film} are smaller for sapphire substrates than for Si substrates, indicating that the stress in the films is also smaller or sapphire. Biaxial stress in thin films is caused by intrinsic stress and external stress. Intrinsic stress is related to defects and impurities. Extrinsic stress is mainly related to lattice and thermal mismatches [26]. The lattice mismatch between the ZnO film and the Si and sapphire substrates is 40% and 18%, respectively [26], [27].

The structural, electrical, and optical properties of AZO thin films fabricated at room temperature with constant RF power and Ar gas pressure depend on the substrate type and film thickness. Focusing on the substrate type, the Si substrates used in this study and the widely used glass substrates have crystallinity similar to that of amorphous glass due to the native oxide on the Si surface [28]. In addition, sapphire substrates and ZnO both have a hexagonal crystal structure, so the AZO thin films with good crystallinity are deposited. In terms of electrical properties, carrier density and Hall mobility are related to crystallinity and bonding state in the film, and thus depend on the substrate type, but are also greatly affected by other factors such as Al addition amount and process conditions. For optical properties, visible light transmittance is related to crystallinity and carrier density, so optimization of deposition conditions is necessary in addition to substrate type. The physical properties of other AZO thin films prepared under sputtering conditions similar to those in this study but using solid targets consisting of ZnO mixed with Al_2O_3 are summarized in Table 2 [17], [24], [29], [30], [31], [32], [33]. References [17], [24], [29], [30] reported film thicknesses similar to the AZO thin films prepared in this study, and comparing the FWHM of the ZnO (002) diffraction peak and crystallite size, the mixed powder target and solid target exhibit similar crystallinity. References [31], [32], [33] in Table 2 show larger deposition rates and film thicknesses than the AZO films in Table 1, and the FWHM of the ZnO (002) diffraction peak is smaller and more crystalline for the solid target than for the powder target. This is because the strain in the film relaxes as the film thickness increases [24].

C. ELECTRICAL PROPERTIES

There is a relationship between the resistivity ρ, carrier density n, charge of carrier e, and Hall mobility μ as shown in the following equation [34]:

$$\rho = \frac{1}{ne\mu}(\Omega\cdot\text{cm}) \tag{4}$$

Fig. 11 shows the resistivity, carrier density, and Hall mobility of AZO films deposited on Si and sapphire substrates, examined by Hall effect measurement. All AZO thin films exhibited n-type behavior. For both the Si and sapphire substrates, the resistivity decreases while the carrier density and Hall mobility increase as the density of the powder target increases. From (4), the decrease in ρ is attributed to the increase in the product of n and μ. In Fig. 11, the lowest resistivities are obtained when the powder target density is 3.00 g/cm^3, resulting in 1.35×10^{-3} Ω·cm, and 1.4×10^{-3}

TABLE 1. Structural Properties OF AZO Thin Films

(a) Si

ρ_{powder} (g/cm^3)	Thickness (nm) (Deposition rate (nm/min))	2θ (deg.)	FWHM (deg.)	c_{film} (Å)	D (nm)	ε_{zz} (%)	σ_{film} (GPa)
0.898	134 (2.24)	34.13	0.623	5.250	13.9	–0.826	1.92
1.28	288 (4.81)	34.23	0.596	5.235	14.6	–0.538	1.25
2.08	314 (5.24)	34.34	0.526	5.219	16.5	–0.231	0.54
3.00	336 (5.60)	34.25	0.558	5.232	15.6	–0.480	1.12

(b) Sapphire

ρ_{powder} (g/cm^3)	Thickness (nm) (Deposition rate (nm/min))	2θ (deg.)	FWHM (deg.)	c_{film} (Å)	D (nm)	ε_{zz} (%)	σ_{film} (GPa)
0.898	121 (2.02)	34.34	0.502	5.219	17.3	–0.231	0.537
1.28	241 (4.01)	34.26	0.483	5.231	18.0	–0.461	1.074
2.08	349 (5.82)	34.29	0.496	5.226	17.8	–0.365	0.850
3.00	372 (6.19)	34.38	0.507	5.213	17.1	–0.115	0.269

TABLE 2. Physical Properties of AZO Thin Films Obtained From Other Reports

Sputtering conditions	Thickness (Deposition rate)	Structural properties	Electrical properties	Optical properties	Ref.
RF 100 W Ar 0.5 Pa RT, glass	250 nm	FWHM = 1.39 deg. D = 6.25 nm σ_{film} ~ 1.125 GPa	$\rho = 5.755\times10^{-1}$ Ω·cm $n \sim 5.75\times10^{21}$ cm^{-3} $\mu \sim 2\times10^{-3}$ cm^2/Vs	$T_{VIS} \sim 90\%$ $E_g = 3.81$ eV	[17]
RF 100 W Ar 0.3 Pa RT, ITO/PET	150 nm	FWHM = 0.325 deg. D = 44.1 nm $\varepsilon_{zz} = -0.064\%$ $\sigma_{film} = 0.149$ GPa	$\rho = 2.03\times10^{-4}$ Ω·cm $n = 3.35\times10^{21}$ cm^{-3} $\mu = 9.150$ cm^2/Vs	$T_{VIS} > 75\%$ $E_g \sim 3.26$ eV	[24]
RF 100 W Ar 0.3 Pa RT, glass	300 nm	FWHM = 0.99 deg. D = 8.16 nm	$\rho = 1.5\times10^{-3}$ Ω·cm	$T_{VIS} \sim 85\%$ $E_g = 3.38$ eV	[29]
RF 165 W Ar 0.4 Pa RT, glass	180 nm (~ 6 nm/min)	FWHM = 0.3877 deg. D = 21.20 nm	$\rho \sim 1.2\times10^{-3}$ Ω·cm	$T_{VIS} = 86.93\%$ $E_g \sim 3.65$ eV	[30]
RF 100 W Ar 0.2 Pa RT, Si, glass	(~ 46 nm/min)	FWHM = 0.39 deg. $\sigma_{film} \sim -0.81$ GPa	$\rho = 2.5\times10^{-3}$ Ω·cm	$E_g \sim 3.38$ eV	[31]
RF 100 W Ar 0.27 Pa RT, glass	~ 990 nm (~ 8.25 nm/min)	FWHM = 0.27 deg.	$\rho = 2.4\times10^{-4}$ Ω·cm	$T_{ave} = 85\%$	[32]
RF 150 W Ar 0.67 Pa 200 °C, sapphire	≤ 500 nm	FWHM ~ 0.38 deg.	$\rho \sim 1.5\times10^{-1}$ Ω·cm $n \sim 5.5\times10^{19}$ cm^{-3} $\mu \sim 9.75$ cm^2/Vs	$T_{550nm} \sim 80\%$	[33]

Ω·cm for Si and sapphire substrates, respectively. From Table 1, the corresponding AZO thin film thicknesses for these resistivities are 336 and 372 nm for Si and sapphire substrates, respectively. These resistivities are similar compared with that of Ref. [29] with 300 nm film thickness, shown in Table 2. Thus, powder targets can be used to prepare AZO thin films with electrical properties comparable to those of solid targets.

D. OPTICAL PROPERTIES

The AZO thin films deposited on sapphire substrates using powder targets with different densities are transparent, and the underlying characters are visible, as shown in Fig. 12. Fig. 13(a) shows the UV-visible light transmission spectra of the AZO thin films. Optical transmittances exceeding 80% in the visible region (wavelength λ = 380–780 nm) are obtained for all AZO thin films. For the film with ρ_{powder} = 0.898 g/cm^3, the optical transmittance near the UV region (λ < 380 nm) is not blocked light completely because the film thickness is thinner [35]. The optical band gap E_g was calculated from the following expression by assuming a direct transition between the valance and conduction bands [36]:

$$(\alpha h\nu)^2 = C\left(h\nu - E_g\right) \tag{5}$$

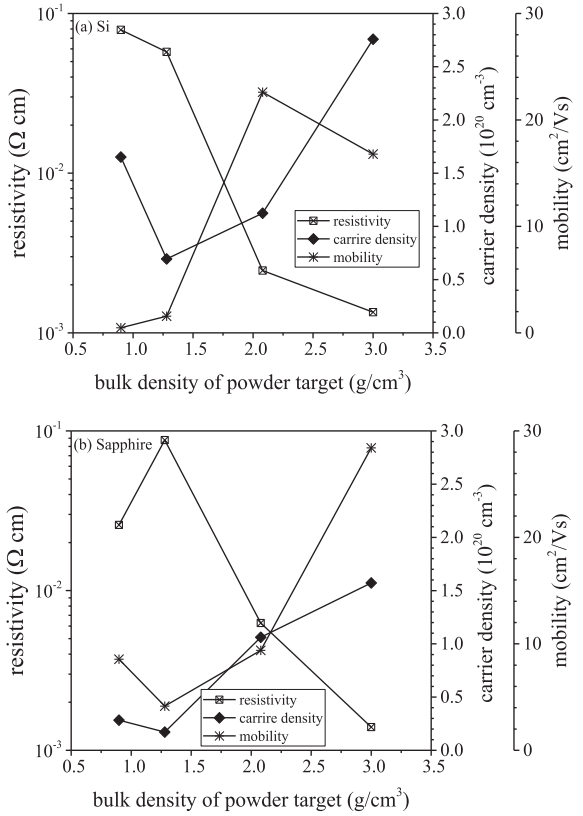

FIGURE 11. **Resistivity, carrier density, and Hall mobility of AZO thin films fabricated on (a) Si and (b) sapphire substrates using powder targets with different bulk densities.**

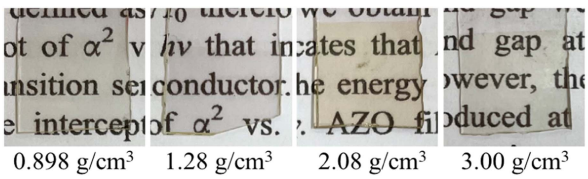

FIGURE 12. **AZO thin films fabricated on sapphire substrates using powder targets of different bulk densities.**

Where α is the optical absorption coefficient, h is Planck's constant, ν is the photon frequency, and C is a constant. The E_g was calculated from a plot of $(\alpha h\nu)^2$ versus the photon energy $h\nu$, as shown in the Tauc plots in Fig. 13(b). The E_g of the AZO thin film increased from 3.21 to 3.38 eV as the bulk density of the powder target increased, as shown in Fig. 13(c). The inset of Fig. 13(c) shows the relationship between the E_g and the carrier density n measured in Fig. 11(b). The shift in E_g is proportional to $n^{2/3}$, which is known as the Burstein–Moss effect [37], [38], [39], [40], [41].

E. FIGURE OF MERIT

To evaluate the suitability of AZO thin films for optoelectronic applications, the optical and electrical properties were combined to calculate the figure of merit (FOM) using the

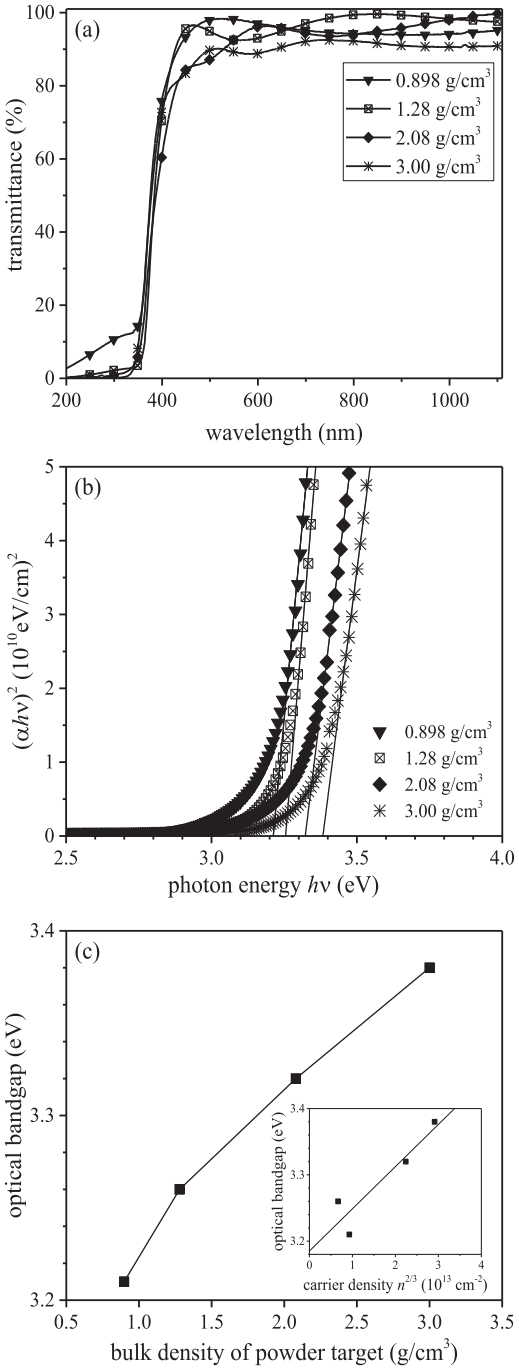

FIGURE 13. **(a) UV-visible light transmission spectra, (b) Tauc plots, and (c) optical band gap values of AZO thin films fabricated on sapphire substrates using powder targets with different bulk densities (inset: optical band gap vs. carrier density).**

following equation [42], [43]:

$$FOM = \frac{T_{VIS}^{10}}{R_s}(\Omega^{-1}) \tag{6}$$

where T_{VIS} and R_s are the average transmittance in the visible region from 380 to 780 nm and the sheet resistance, respectively. Fig. 14 shows the FOM calculated from T_{VIS} and R_s

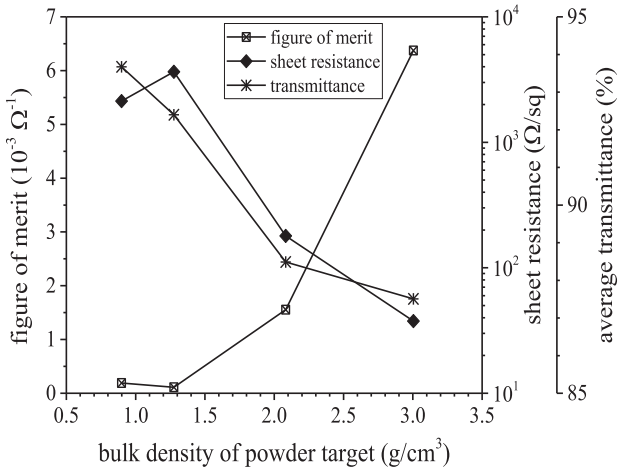

FIGURE 14. FOM, sheet resistance, and average transmittance of visible light (380–780 nm) for AZO thin films fabricated on sapphire substrates using powder targets of different bulk densities.

to determine the optimum bulk density of the powder target. As the bulk density increased, the average visible light transmission decreased from 93.7 to 87.5%. This is due to the film thickness effect and increased scattering, reflection, and light absorption as the film thickness increases [44], [45]. The FOM values significantly increase from 0.112×10^{-3} to 6.37×10^{-3} Ω^{-1} because of the decrease in R_s. This indicates that the R_s of AZO films strongly affects the FOM value, although the T_{VIS} slightly decreases [46]. An optimum FOM value of 6.37×10^{-3} Ω^{-1} has been obtained for AZO thin films prepared using powder targets with a bulk density of 3.00 g/cm^3. This value is comparable to or higher than those reported in other studies [47], [48], [49]. Therefore, the AZO thin films prepared in this study are suitable for optoelectronic device applications.

V. CONCLUSION

Compared with solids, powders involve a larger number of available elements, a greater number of elemental combinations, and more precise control of composition ratios. Therefore, more unknown multicomponent targets can be applied to the sputtering method more easily using powder targets, which is effective for the development of new functional materials. In this study, the author fabricated thin films by sputtering using powder targets with different bulk densities. This was achieved by considering that the bulk density changes depending on the pressing pressure during the powder target fabrication process. As a result, all the fabricated AZO thin films showed crystal growth in the ZnO (002) plane, perpendicular to the substrate. The lowest resistivity and highest carrier density and mobilities were obtained when the bulk density of the powder target was highest, 3.00 g/cm^3. For these conditions, the optimal resistivity, carrier density, and Hall mobility were 1.35×10^{-3} Ω·cm, 2.76×10^{20} cm^{-3}, and 28.4 cm^2/Vs, respectively. The optical band gap value of 3.38 eV was the highest when the bulk density was 3.00 g/cm^3. These properties are comparable to those of solid targets, demonstrating that powder targets can be used for sputtering in practical applications.

Notably, the results suggest that the difference in bulk density is related to the flatness of the powder target surface and the behavior of the sputtered particles changes depending on where the Ar ions enter the surface irregularities. The author also investigated the porosity of the powder target by measuring the ratio of the bulk density of the powder target to the theoretical solid density, but the results were not sufficiently accurate. In the future, we will investigate the effects of the surface morphology and porosity of the powder target on the sputtering performance and deposited film properties.

ACKNOWLEDGMENT

Tamiko Ohshima is grateful to Professor Hiroharu Kawasaki, Lecture Yusuke Hibino, Professor Yoshihito Yagyu, Associated Professor Takeshi Ihara, and Assistant Professor Takahiko Satake of the National Institute of Technology, Sasebo College for their help in conducting this research.

REFERENCES

[1] W. G. Suci, H. K. Aliwarga, Y. R. Azinuddin, R. B. Setyawati, K. N. R. Stulasti, and A. Purwanto, "Review of various sulfide electrolyte types for solid-state lithium-ion batteries," *Open Eng.*, vol. 12, pp. 409–423, Jun. 2022.

[2] H. Nagata and J. Akimoto, "All-oxide solid-state lithium-ion battery employing $50Li_2SO_4$–$50Li_2CO_3$ glass electrolyte," *J. Power Sources*, vol. 491, Apr. 2021, Art. no. 229620.

[3] Preparation Meeting for Formulation of Strategies for Enhancing Material Innovation Power Toward., "*Toward government strategies for enhancing material innovation power*," Jun. 2020. [Online]. Available: https://www.mext.go.jp/content/20200818-mxt_nanozai-000007028_11.pdf

[4] H. Kawasaki, T. Ohshima, Y. Yagyu, T. Ihara, R. Tanaka, and Y. Suda, "Preparation of tris (8-hydroxyquinolinato) aluminum thin films by sputtering deposition using powder and pressed powder targets," *Jpn. J. Appl. Phys.*, vol. 56, Apr. 2017, Art. no. 06HE01.

[5] T. Ohshima et al., "Sputtering deposition of Al-doped zinc oxide thin films using mixed powder targets," *J. Appl. Phys.*, vol. 55, Nov. 2015, Art. no. 01AA08.

[6] D. Depla, "Sputtering deposition with powder targets: An overview," *Vacuum*, vol. 184, Nov. 2021, Art. no. 109892.

[7] S. Takaki, "The present and challenges of transparent conductive film," *J. Vac. Soc. Jpn.*, vol. 50, pp. 105–110, 2007.

[8] D. K. Kim and H. B. Kim, "Room temperature deposition of Al-doped ZnO thin films on glass by RF magnetron sputtering under different Ar gas pressure," *J. Alloys Compounds*, vol. 509, pp. 421–425, Jan. 2011.

[9] L. S. Ning, Z. Y. Wen, S. T. Yi, and W. F. Yu, "Fabrication and characterization of the AZO/Ag/AZO transparent conductive films prepared by RF magnetron sputtering using powder targets," *Nanoscience Nanotechnol. Lett.*, vol. 7, pp. 743–748, Sep. 2015.

[10] A. Tanaka et al., "Review of pulmonary toxicity of indium compounds to animals and humans," *Thin Solid Films*, vol. 518, pp. 2934–2936, 2010.

[11] S. Niki, K. Matsubara, H. Tampo, and K. Nakahara, "ZnO-based transparent conducting oxide films," *J. Vac. Soc. Jpn.*, vol. 50, pp. 114–117, 2007.

[12] P. J. Kelly, Y. Zhou, and A. Postill, "A novel technique for the deposition of aluminium-doped zinc oxide films," *Thin Solid Films*, vol. 426, pp. 111–116, Feb. 2003.

[13] B. Khalfallah, F. Chaabouni, G. Schmerber, A. Dinia, and M. Abaab, "Investigation of physico-chemical properties of conductive Ga-doped ZnO thin films deposited on glass and silicon wafers by RF magnetron sputtering," *J. Mater. Sci.: Mater. Electron.*, vol. 28, pp. 75–85, Jan. 2017.

[14] G. J. Lee, D. K. Lee, and S. H. Sohn, "Thermal annealing effects on the characteristics of transparent semiconducting Zn_2SnO_4 thin films prepared by RF-magnetron sputtering with powder target," *Mol. Crystals Liquid Crystals*, vol. 586, pp. 179–187, Jan. 2014.

[15] F. Y. Wu, J. W. Li, Y. Qi, W. T. Ding, Y. Y. Guo, and Y. W. Zho, "Characteristics of the structure and properties of $ZnSnO_3$ films by varying the magnetron sputtering parameters," *Acta Metallurgica Sinica*, vol. 29, pp. 827–833, Sep. 2016.

[16] B. A. Mangour, "Powder metallurgy of stainless steel: State-of-the art, challenges, and development," in *Stainless Steel: Microstructure, Mechanical Properties and Methods of Application*, A. Pramanik and A. K. Basak Eds. New York, NY, USA: Nova Sci. Publishers, 2015, pp. 37–80.

[17] J. Chen et al., "Preparation and characterization of high-transmittance AZO films using RF magnetron sputtering at room temperature," *Appl. Surf. Sci.*, vol. 317, pp. 1000–1003, Oct. 2014.

[18] P. R. Kalvani, S. Shapouri, A. R. Jahangiri, and Y. S. Jalili, "Microstructure evolution in high density AZO ceramic sputtering target fabricated via multistep sintering," *Ceram. Int.*, vol. 46, pp. 5983–5992, Apr. 2020.

[19] T. Ishida, "Preparing conductive transparent ITO film by RF magnetron sputtering with low self bias and study on its self bias," *J. Vac. Soc. Jpn.*, vol. 44, pp. 747–750, Jul. 2001.

[20] T. Sugawara, Y. Taya, I. Shimono, and I. Suga, "Measurement of self-bias voltage on radio-frequency magnetron sputtering," *Res. Rep. Hokkaido Ind. Technol. Center*, vol. 6, pp. 45–47, 2000.

[21] F. Boydens, W. P. Leroy, R. Persoons, and D. Depla, "The influence of target surface morphology on the deposition flux during direct-current magnetron sputtering," *Thin Solid Films*, vol. 531, pp. 32–41, Mar. 2013.

[22] H. P. Klug and L. E. Alexander, *X-ray Diffraction Procedures: For polycrystalline and amorphous materials*. New York, NY, USA: Wiley, 1974.

[23] R. Cebulla, R. Wendt, and K. Ellmer, "Al-doped zinc oxide films deposited by simultaneous RF and dc excitation of a magnetron plasma: Relationships between plasma parameters and structural and electrical film properties," *J. Appl. Phys.*, vol. 83, pp. 1087–1095, Jun. 1998.

[24] N. Akin, S. S. Cetin, M. Cakmak, T. Memmedl, and S. Ozcelik, "Effect of film thickness on properties of aluminum doped zinc oxide thin films deposition on polymer substrate," *J. Mater. Sci: Mater. Electron.*, vol. 24, pp. 5091–5096, Oct. 2013.

[25] Y. F. Li et al., "Characterization of biaxial stress and its effect on optical properties of ZnO thin films," *Appl. Phys. Lett.*, vol. 91, Jul. 2007, Art. no. 021915.

[26] P. Wang et al., "Quality improvement of ZnO thin layers overgrown on Si(100) substrates at room temperature by nitridation pretreatment," *AIP Adv.*, vol. 2, Jun. 2012, Art. no. 022139.

[27] N. Itagaki et al., "Growth of single crystalline films on lattice-mismatched substrates through 3D to 2D mode transition," *Sci. Rep.*, vol. 10, Mar. 2020, Art. no. 4669.

[28] L. Wen, B. B. Sahu, H. R. Kim, and J. G. Han, "Study on the electrical, optical, structural, and morphological properties of highly transparent and conductive AZO thin films prepared near room temperature," *Appl. Surf. Sci.*, vol. 473, pp. 649–656, Apr. 2019.

[29] J. R. Ray, M. S. Desai, C. J. Panchal, and P. B. Patel, "Magnetron sputtered Al-ZnO thin films for photovoltaic applications," *J. Nano-Electron. Phys.*, vol. 3, pp. 755–765, Jan. 2011.

[30] S. N. E. Duygulu, A. O. Kodolbas, and A. Ekerim, "Effects of argon pressure and RF power on magnetron sputtered aluminum doped ZnO thin films," *J. Cryst. Growth*, vol. 394, pp. 116–125, May 2014.

[31] S. Rahmane, M. A. Djouadi, M. S. Aida, N. Barreau, B. Abdallah, and N. H. Zoubir, "Power and pressure effects upon magnetron sputtered aluminum doped ZnO films properties," *Thin Solid Films*, vol. 519, pp. 5–10, Oct. 2010.

[32] J. Yoo et al., "High transmittance and low resistive ZnO:Al films for thin film solar cells," *Thin Solid Films*, vol. 480, pp. 213–217, Jun. 2005.

[33] K. Yim, H. Kim, and C. Lee, "Effects of the O2/Ar gas flow ratio on the electrical and transmittance properties of ZnO: Al films deposited by RF magnetron sputtering," *J. Electroceramics*, vol. 17, pp. 875–877, Dec. 2006.

[34] A. C. Badgujar, B. S. Yadav, G. K. Jha, and S. R. Dhage, "Room temperature sputtered aluminum-doped ZnO thin film transparent electrode for application in solar cells and for low-band-gap optoelectronic devices," *ACS Omega*, vol. 7, pp. 14203–14210, Apr. 2022.

[35] S. H. Seo and H. C. Kang, "Growth of ZnO/sapphire heteroepitaxial thin films by radio-frequency sputtering with a raw powder target," *Thin Solid Films*, vol. 518, pp. 5164–5168, Jul. 2010.

[36] X. L. Zhang, K. S. Hui, and K. N. Hui, "High photo-responsivity ZnO UV detectors fabricated by RF reactive sputtering," *Mater. Res. Bull.*, vol. 48, pp. 305–309, Feb. 2013.

[37] T. Oyama, "Transparent conductive film: Current status and future trend," *J. Surf. Finishing Soc. Jpn.*, vol. 60, pp. 616–621, Oct. 2009.

[38] S. C. Dixon, D. O. Scanlon, C. J. Carmalt, and I. P. Parkin, "n-Type doped transparent conducting binary oxides: An overview," *J. Mater. Chem. C*, vol. 4, pp. 6946–6961, Aug. 2016.

[39] H. Benzarouk et al., "Effect of different dopant elements (Al, Mg and Ni) on microstructural, optical and electrochemical properties of ZnO thin films deposited by spray pyrolysis (SP)," *Superlattices Microstructures*, vol. 52, pp. 594–604, Sep. 2012.

[40] T. Haranou and S. Takaki, "A review of typical properties indium-tin oxide films," *J. Surf. Finishing Soc. Jpn.*, vol. 40, pp. 666–670, May 1989.

[41] K. G. Saw, N. M. Aznan, F. K. Yam, S. S. Ng, and S. Y. Pung, "New insights on the Burstein-Moss shift and band gap narrowing in indium-doped zinc oxide thin films," *PLoS One*, vol. 10, Oct. 2015, Art. no. e0141180.

[42] B. N. Q. Trinh, T. D. Chien, N. Q. Hoa, and D. H. Minh, "Solution-processable zinc oxide based thin films with different aluminum doping concentrations," *J. Sci.: Adv. Mater. Devices*, vol. 5, pp. 497–501, Dec. 2020.

[43] G. Haacke, "New figure of merit for transparent conductors," *J. Appl. Phys.*, vol. 47, pp. 4086–4089, Sep. 1976.

[44] B. L. Zhu, J. Wang, S. J. Zhu, J. Wu, D. W. Zeng, and C. S. Xie, "Thickness study of AZO films by RF sputtering in $Ar + H_2$ atmosphere at room temperature," *Physica Status Solidi*, vol. 209, pp. 1251–1258, Apr. 2012.

[45] B. L. Zhu, S. J. Zhu, J. Wang, J. Wu, D. W. Zeng, and C. S. Xie, "Thickness effect on structure and properties of ZAO thin films by RF magnetron sputtering at different substrate temperature," *Physica E*, vol. 43, pp. 1738–1745, Jul. 2011.

[46] J. H. Kim et al., "The effects of film thickness on the electrical, optical, and structural properties of cylindrical, rotating, magnetron-sputtered ITO films," *Appl. Surf. Sci.*, vol. 440, pp. 1211–1218, May 2018.

[47] B. Sarma, D. Barman, and B. K. Sarma, "AZO (Al:ZnO) thin films with high figure of merit as stable indium free transparent conducting oxide," *Appl. Surf. Sci.*, vol. 479, pp. 786–795, Jun. 2019.

[48] K. D. A. Kumar et al., "Evaluation of the structural, optical and electrical properties of AZO thin films prepared by chemical bath deposition for optoelectronics," *Solid State Sci.*, vol. 78, pp. 58–68, Apr. 2018.

[49] M. Mohamedi et al., "Role of substrate and annealing on microstructural, optoelectronic and luminescence properties of RF magnetron sputtered AZO thin films in confocal configuration," *J. Lumin.*, vol. 244, Apr. 2022, Art. no. 118739.